Structural and electronic properties of isovalent boron atoms in GaAs

C. M. Krammel,[1,a)] L. Nattermann,[2] E. Sterzer,[2] K. Volz,[2] and P. M. Koenraad[1]
[1]*Department of Applied Physics, Eindhoven University of Technology, Eindhoven 5612 AZ, The Netherlands*
[2]*Materials Science Center and Faculty of Physics, Philipps-Universität Marburg, 35032 Marburg, Germany*

(Received 30 October 2017; accepted 21 December 2017; published online 9 February 2018)

Boron containing GaAs, which is grown by metal organic vapour phase epitaxy, is studied at the atomic level by cross-sectional scanning tunneling microscopy (X-STM) and spectroscopy (STS). In topographic X-STM images, three classes of B related features are identified, which are attributed to individual B atoms on substitutional Ga sites down to the second layer below the natural {110} cleavage planes. The X-STM contrast of B atoms below the surface reflects primarily the structural modification of the GaAs matrix by the small B atoms. However, B atoms in the cleavage plane have in contrast to conventional isovalent impurities, such as Al and In, a strong influence on the local electronic structure similar to donors or acceptors. STS measurements show that B in the GaAs {110} surfaces gives rise to a localized state short below the conduction band (CB) edge while in bulk GaAs, the B impurity state is resonant with the CB. The analysis of $B_xGa_{1-x}As$/GaAs quantum wells reveals a good crystal quality and shows that the incorporation of B atoms in GaAs can be controlled along the [001] growth direction at the atomic level. Surprisingly, the formation of the first and fourth nearest neighbor B pairs, which are oriented along the ⟨110⟩ directions, is strongly suppressed at a B concentration of 1% while the third nearest neighbor B pairs are found more than twice as often than expected for a completely spatially random pattern. *Published by AIP Publishing.*
https://doi.org/10.1063/1.5011166

I. INTRODUCTION

Alloying binary III-V compounds with isovalent impurities is a common method to tailor their material properties. Historically, this was primarily done by introducing isovalent atoms, which are very similar in terms of size and electronegativity, to the substituted species in the host material. The electronic properties of these "conventional" (Al, Ga, In) (P, As, Sb) alloys, such as the band gap and effective mass, can generally be well described by the linear interpolation between the binary end points with a small bowing parameter, which is known as the virtual crystal approximation (VCA). Progress in state-of-the-art growth technology has led to a growing interest in alloying conventional binary III-V compounds with highly mismatched isovalent impurities, which were previously problematic to synthesize. The large disparity between the isovalent impurity and host material represents in the case of highly mismatched alloys (HMAs), a strong perturbation of the host states, which fundamentally changes the nature of the impurity host interactions. This offers new functionalities, which are often described within the phenomenological band anticrossing (BAC) model.[1,2] Prominent examples are the extensively studied dilute nitrides[3–5] and the relatively new dilute bismides,[6–9] which are currently attracting a lot of attention. So far, HMAs in the III-V material system have only been formed by alloying on the anionic sublattice. In view of this, it is from a fundamental perspective interesting to investigate a HMA with mixed cation elements.

A potential candidate for such a highly mismatched cation alloy is B doped GaAs. However, there is an ongoing discussion due to conflicting reports in literature whether (B,Ga)As is truly a HMA. On the one hand, boron is an element in the second row of the periodic table and has next to N atoms, the second smallest covalent radius in the III-V system.[10] This gives rise to a considerable difference in the effective sizes of B and Ga, which is typical for a HMA. On the other hand, the electronegativities of B and As atoms are very similar, which leads in the III-V system to the unique situation of an almost exclusively covalent B-As bond with very weak ionic contributions. In that sense, boron in GaAs is neither a conventional nor a highly mismatched impurity. This ambivalence continues in the electronic properties of B doped GaAs. For example, the band gap of GaAs shows a nearly linear blue shift upon B incorporation, which can be described by a relatively small and composition independent bowing parameter of ≈3.5 eV.[11,12] Such a behavior is typical for "conventional" amalgamation like alloys. In contrast, the boron incorporation leads to a huge increase in the effective mass of the conduction band (CB).[13] A similar behavior has been reported for dilute nitrides, which are the best studied HMAs in the III-V system. Both the VCA and the BAC model cannot fully describe the unusual electronic properties of B doped GaAs. This shows that a fundamental understanding of the interactions between the B atoms and the GaAs host is largely lacking, which requires detailed knowledge about the structural and electronic properties at the atomic level.

Experimentally, it is very challenging to probe the influence of the B atoms on the local electronic structure of GaAs. The B related states, despite being located in the s-like CB, possess a strong p-like character.[14] This implies that optical transitions between the B states and the likewise

a)Electronic mail: c.m.krammel@tue.nl

p-like valence band (VB) states are dipole forbidden, which represents a fundamental limitation for optical analysis techniques. Magnetotransport measurements under hydrostatic pressure can provide an indication for the average B related density of states (DOS).[15–17] These measurements suggest that the states of isolated B atoms and B clusters, which can act as isovalent charge carrier traps, are located in the region of the CB. However, the interpretation of pressure dependent magnetotransport measurements is rather challenging due to a lack of structural information.

In this paper, we use cross-sectional scanning tunneling microscopy (X-STM) to study the structural and electronic properties of isovalent boron atoms in GaAs. The growth of the sample and the X-STM measurement are described in Sec. II. The main B related features, found in the X-STM measurements, are first classified in Sec. III A. Thereafter, the electronic properties of an individual B atom in one of the GaAs {110} surfaces are investigated in Sec. III B. In addition, the structural properties of $B_xGa_{1-x}As$/GaAs quantum wells (QWs) with B concentrations ranging from 0.3% to 1.0% are examined in Sec. III C. Finally, in Sec. IV, a summary of our work is presented.

II. EXPERIMENTAL

One dedicated X-STM sample is investigated, which contains three different groups of $B_xGa_{1-x}As$/GaAs QWs with nominal B concentrations of 0.3% (QWs 1), 0.5% (QWs 2), and 1% (QWs 3). The investigated sample was grown with metal organic vapour phase epitaxy (MOVPE) in a commercially available horizontal reactor system Aixtron AIX-200 with gas flow rotation. For the deposition of the GaAs and $B_xGa_{1-x}As$ layers, Pd purified H_2 (10 N) was utilized as the carrier gas under a reduced reactor pressure of 50 mbar. Triethylgallium (TEGa), tertiarybutylarsine (TBAs), and triethylboron (TEB) were used as metal organic sources. A standard n-type GaAs wafer served as the basis for the growth. First, a 250 nm GaAs buffer layer was grown at 625 °C on top of the substrate to provide perfect surface conditions for the growth of the $B_xGa_{1-x}As$ layers. Afterwards, the growth temperature was decreased to 575 °C. Starting with the lowest composition of 0.3%, three 15 nm wide $B_xGa_{1-x}As$ QWs were grown, which were separated by 20 nm wide GaAs barriers. A further group of three $B_xGa_{1-x}As$/GaAs QWs with a B concentration of 0.5% was grown after a 60 nm wide GaAs space layer. This scheme was repeated once more for the last set of $B_xGa_{1-x}As$/GaAs QWs with a B concentration of 1.0%. At the end of the growth, the epilayer region was capped by a 50 nm thick GaAs layer.

The X-STM measurements were performed in a conventional Omicron low-temperature STM at about 5 K. The samples were cleaved *in situ* under ultra-high vacuum (UHV) conditions at a base pressure below 4×10^{-11} mbar revealing one of the natural {110} cleavage planes. Tips were made from polycrystalline tungsten wires by electrochemical etching followed by baking and Ar-sputtering steps in the UHV system of the STM. All shown filled and empty state X-STM images were acquired in the constant current mode.

III. RESULTS AND DISCUSSION

A. Classification of the main boron related features

Up to now, X-STM has hardly been used to study B doped III-V semiconductor compounds. A first indication of the structural and electronic properties of B atoms in and below the natural {110} cleavage planes is provided by voltage-dependent topographic X-STM measurements of the same area. Figure 1 shows a series of selected empty and filled state images of QW 1 with a B content of 0.3%, which cover a wide range of positive and negative voltages. Here, three different classes of B related features (0, 1, 2) can be identified. The appearance of these B related features depends strongly on the sample bias, which points to variable contributions from both electronic and topographic effects. This is most pronounced for class (0) whose appearance ranges from a dark atomic-like object to an extended bright

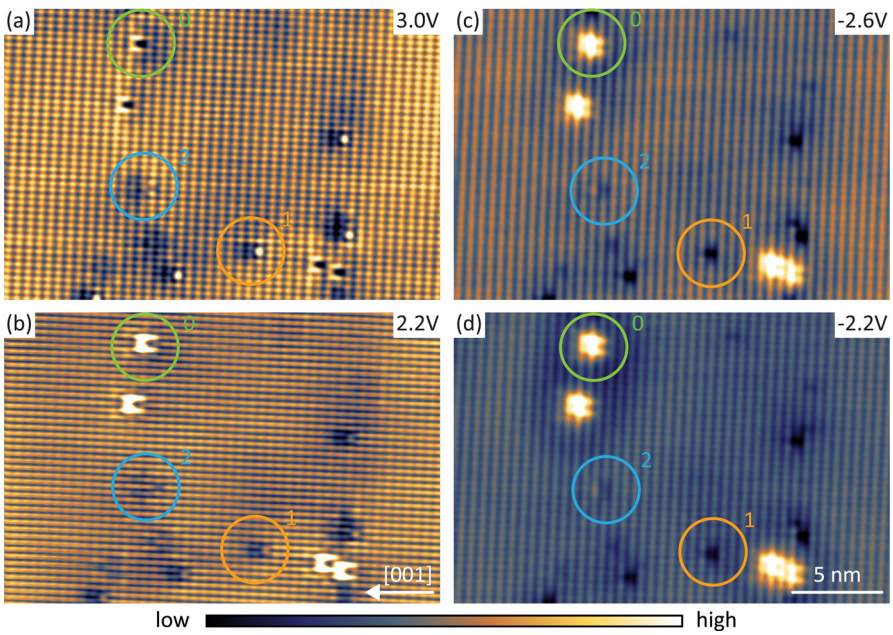

FIG. 1. Typical topographic X-STM images of the same area of QW 1 with a B content of 0.3%. In the first column, topographic empty state images are shown, which are taken at large (a) and small (b) positive voltages. The second column represents topographic filled state images, which are acquired at large (c) and small (d) negative voltages. Three different classes of B related features (0, 1, 2) can be distinguished, which are attributed to B atoms down to the second layer below the {110} cleavage planes. The tunnel current is in all cases set to $I = 30$ pA. The color ranges of the STM images are independently adjusted for best visibility and the [001] growth direction is indicated by a white arrow.

feature. Classes (1) and (2) also undergo changes, but are primarily dominated by local dark components.

Likewise, the corrugation in Fig. 1, which is determined by the symmetry of the surface states involved in the tunneling process, depends on the sample voltage. On cleaved {110} surfaces of zinc-blende III-V semiconductors, STM has access to two types of surface states, which are either localized on the cationic (C_3, C_4) or anionic (A_4, A_5) sublattice.[18] The cationic C_3 state is energetically located in the region of the conduction band edge (CBE) and extends along the [001] direction. The C_4 state, which lies deeper in the CB, extends perpendicular to the C_3 state along the $[\bar{1}10]$ direction. This explains the transition from a one- to a two-dimensional corrugation when tunneling at higher positive voltages into states deeper in the CB [see Figs. 1(a) and 1(b)]. Conversely, the anionic states A_5 and A_4, which lie at different depths in the VB, extend both along the $[\bar{1}10]$ direction. Therefore, the atomic corrugation in Figs. 1(c) and 1(d) is unchanged at negative voltages. This is an important observation for the interpretation of the B related features in Fig. 1 as it excludes contributions from the VB/CB at positive/negative voltages.

The structural effects of the B atoms on the GaAs {110} surfaces can be understood with the help of a geometrical model, which is based on the covalent radii of the isovalent impurity and the atoms in the host. Tilley *et al.* have shown in Ref. 19 that it is possible to reliably predict in an analytic way the positions of all group III and V dopants in the GaAs (110) surface with respect to fully relaxed DFT calculations. In addition, we have recently demonstrated that the structural modifications of the {110} surfaces by Bi atoms down to the second layer can be detected in topographic X-STM measurements.[20] In filled state X-STM images, which are taken at a high negative sample voltage, the large Bi atoms in even or odd numbered layers lead to a displacement of either one or a rectangle of four atoms out of the surface. Similar observations have been made for small N atoms, which give rise to local depressions in the surface with the same symmetry as for Bi.[21–23] Hence, the local dark contributions at classes (0, 1, 2) must be related to structural modifications of the GaAs surface by the smaller B atoms. Conversely, this suggests that the bright contributions to the contrast are related to changes in the DOS.

The examples of Bi and N show that it is possible to deduce the position of the impurity atom in the lattice from the symmetry and strength of the structural modifications. High resolution filled and empty state images, which provide complementary information on solely the anionic or cationic sublattices, as in the case of Fig. 1, are in this regard essential. The topographic effects are best visible in the filled and empty state images in Figs. 1(a) and 1(c), which are taken at large positive and negative voltages. Magnified portions of the areas highlighted in these images are shown in Fig. 2 in combination with a three-dimensional model of the relaxed (110) surface. Boron can be incorporated on cationic or anionic lattice positions, where it acts as an isovalent impurity or an acceptor, respectively. This crucially depends on the growth parameters. Under group V rich growth conditions, as used in the investigated sample, isovalent incorporation on cationic positions is strongly favored.[15–17]

The covalent radius of B ($r_B = 85$ pm) is much smaller than the covalent radii of Ga ($r_{Ga} = 124$ pm) and As ($r_{As} = 121$ pm) in the surrounding matrix.[10] This means the covalent B-As bonds are shorter than the covalent Ga-As bonds, $r_B + r_{As} < r_{Ga} + r_{As}$, which locally deforms the surrounding GaAs matrix towards the B impurity. The DFT calculations in Ref. 19 show that a B atom in the cleavage plane relaxes as a result of the shorter bond length into a deeper position where it lies below the surrounding Ga atoms. The displacement leads to a reduced tunnel probability at the same height above the B atom, which is predicted to give rise to an

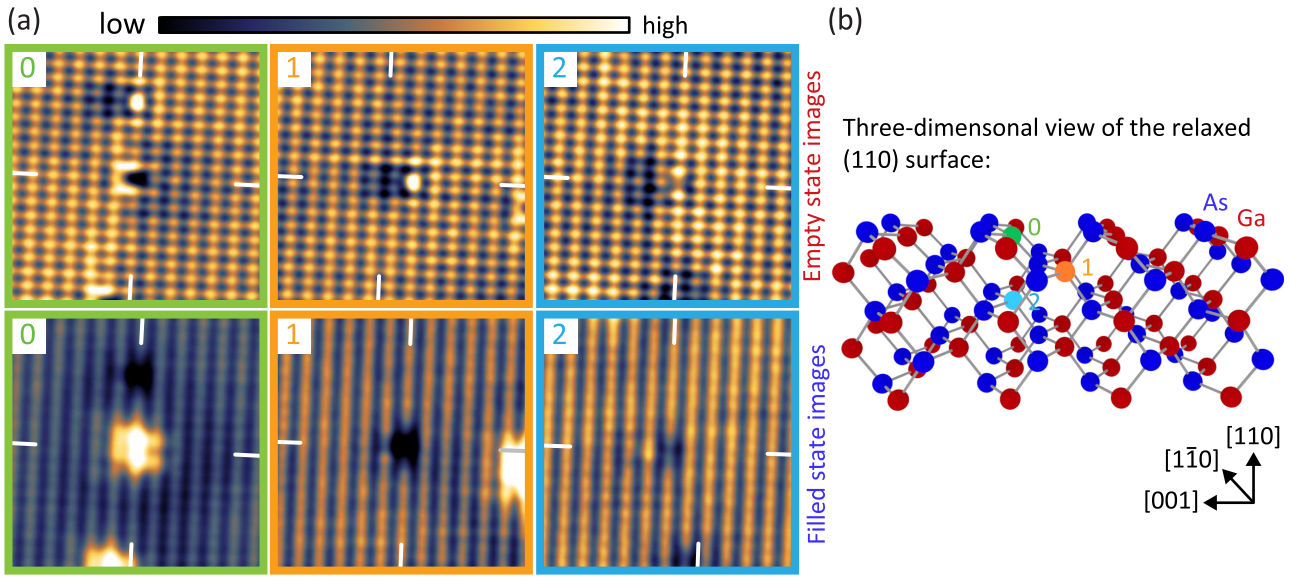

FIG. 2. Discussion of the structural effects of B atoms in layers 0, 1, and 2 on the relaxed GaAs {110} surfaces. The structural modifications, which appear as dark regions, are most apparent in the filled and empty state images in Figs. 1(a) and 1(c). Magnified portions of the areas marked in these images are shown in (a). Cross-hairs indicate the position of the features' center with respect to the atomic corrugation. A three-dimensional model of the relaxed (110) surface is provided in (b), where the positions of classes (0, 1, 2) are marked.

atomic-like depression in an empty state X-STM image.[19] This is in good qualitative agreement to the experimental empty state X-STM image in Fig. 2(a) of class (0), which is taken at a large positive sample voltage. In addition, the B atom in the surface has direct bonds with two As atoms in the same layer. These two As atoms are equally shifted towards the deeper lying B atom. In a filled state X-STM image, this is expected to give rise to a reduced contrast on two neighboring As corrugation maxima.[19] However, in the experimental filled state X-STM images, a B atom in the surface [class (0)] appears as a bright feature which extends over several lattice sites. This bright contrast is in contradiction to the lower position of the As atoms in the surface and must therefore be an electronic effect. A detailed discussion of the influence of a single B atom in the surface [class (0)] on the local DOS of the GaAs host material is provided in Sec. III B.

A boron atom in the first layer below the surface has a direct bond to one As atom in the surface, which is expected to relax into a lower position due to the shorter B-As bond. Similarly, class (1) appears as an atomic-like depression in the filled state image in Fig. 2(a). In addition, the attractive deformation potential of the B atom in layer one is supposed to give rise to a downward displacement of four Ga atoms in the surface. It is likely that the asymmetry given by the surface relaxation leads to an imbalance between the two neighboring zigzag rows in the cleavage plane. These expectations are in good agreement with the empty state X-STM image of class (1) in Fig. 2(a), which shows an asymmetric reduction of the contrast on four corrugation maxima. The additional bright feature next to the rectangle of four dark corrugation maxima is attributed to changes in the DOS.

The structural modifications of the surface by a B atom two atomic layers deeper are, compared to higher lying B atoms, supposed to further diminish. The strongest effects on the cleavage plane are expected directly above the B atom in the second layer below the surface. This means primarily one Ga and its two neighboring As atoms relax into a lower position with respect to their surrounding. This is conceptually in good agreement with the weak features of class (2) in Fig. 2(a). Here, one corrugation maximum is completely suppressed in the empty state X-STM image, while the contrast is reduced on two neighboring Ga sites in the filled state X-STM image.

All three classes of B related features are found equally often in large stretches of OWs 1–3. In addition, the concentrations of each individual class with respect to one mono atomic layer match well to the intended B content in the QWs. This gives further evidence that classes (0, 1, and 2) are indeed related to individual B atoms down to the second layer below the surface.

B. Boron induced modifications of the local electronic structure

We are turning now to the influence of B on the local density of states (LDOS) of the host, which leads to additional bright contributions in topographic X-STM images, unlike the previously discussed structural effects. The topographic X-STM images in Fig. 1 show that B atoms in the surface [class (0)] have a much stronger influence on the local electronic structure than in subsurface layers [classes (1) and (2)]. To investigate this, spectroscopic measurements are performed on a B atom in the cleavage plane, which is shown in Fig. 3(a).

In a $5 \times 5\text{nm}^2$ large region, individual differential conductance curves, $dI/dU(U,\boldsymbol{r})$, are recorded on a regular grid consisting of 2500 positions. The $dI/dU(U,\boldsymbol{r})$ spectra as a function of the position, $\boldsymbol{r}$, and the voltage, U, are acquired with an open feedback loop after having approached the surface by an additional 0.12 nm to increase the strength of the signal. All $dI/dU(U,\boldsymbol{r})$ spectra consist of 351 values distributed over a voltage range from –2.0 V to 1.5 V. Each $dI/dU(U,\boldsymbol{r})$ point is acquired by a lock-in technique using a carrier wave with an amplitude of $U_{\text{mod}} = 30\,\text{mV}$ and a frequency of $f = 1042\,\text{Hz}$. In between the $dI/dU(U,\boldsymbol{r})$ spectra, the tip is stabilized at a tunnel current of $I = 30\,\text{pA}$ and a voltage of $U = -2.2\,\text{V}$. The corresponding topograph is shown in Fig. 3(a), which is recorded in the back-trace of the tip during the $dI/dU(U,\boldsymbol{r})$ map. The changes of the tip-sample distance, which cannot be avoided for a B atom in the surface, can give rise to topographic crosstalk in the $dI/dU(U,\boldsymbol{r})$ map. This is due to the additional dependence of the differential conductance on the tip-sample distance. A larger/smaller tip sample distance leads to an underestimation/overestimation of the LDOS and thus to an effectively lower/higher differential conductance.[24] However, no significant indications for such a behavior are found in our measurement.

The influence of the B atom in the surface on the local electronic structure can be visualized by subtracting the contribution from the GaAs matrix, which is estimated by averaging over the all $dI/dU(U,\boldsymbol{r})$ spectra in the green framed region of the X-STM image. In that area, the LDOS is not affected by the B atom. A three-dimensional representation of the B related differential conductance, where values below 0.55a. u. are clipped, is shown in Fig. 3(d). This provides a direct image of the B impurity state. Interestingly, the B atom gives rise to three regions of enhanced differential conductivity, one at positive [region (I)] and two at negative [regions (II) and (III)] voltages. In all three cases, the enhancement of the differential conductance is the strongest at two neighboring lobes. This is in good agreement with the topographic filled and empty state images of the B impurity state in Fig. 4.

Corresponding color maps of the B related differential conductance are shown in Fig. 3(c). Cuts 1 and 2, which are perpendicular to each other, have been placed in such a way that they cross in region (I) through one of the two lobes. This illustrates that regions (I) and (II) are both characterized by a steep rise in the differential conductance, which results in a narrow local maximum. The local maxima of regions (I) and (II) are located at the same spatial position and have similar lateral extensions. In contrast, region (III) shifts laterally as the negative voltage increases.

Figure 3(b) shows typical $dI/dU(U,\boldsymbol{r})$ curves of the B atom and the surrounding GaAs matrix. The spectrum of the B atom is determined by averaging over a small region around the crossing of cuts 1 and 2 in Fig. 3(a). The average of all $dI/dU(U,\boldsymbol{r})$ spectra in the green framed region is used

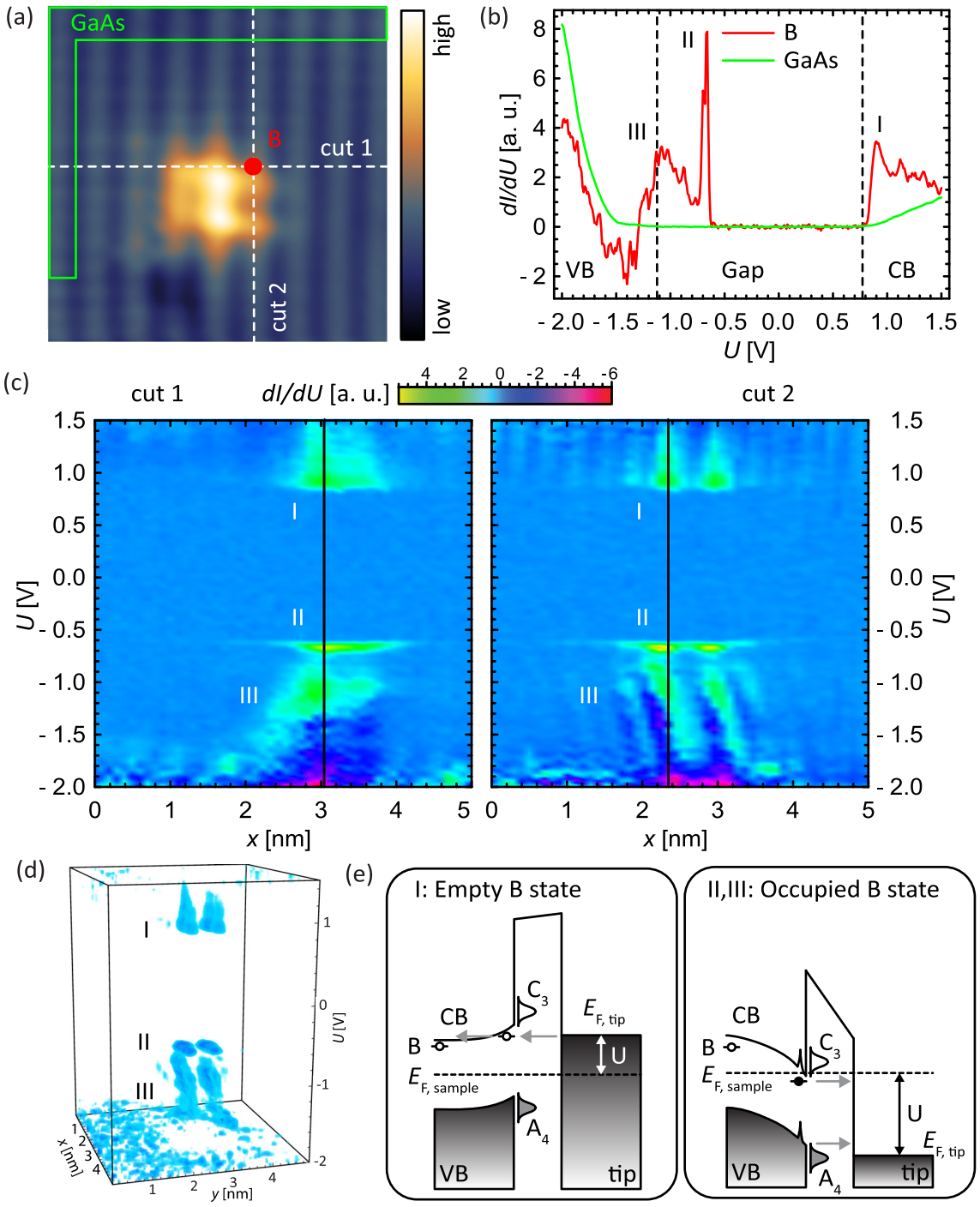

FIG. 3. Spectroscopic analysis of a B atom in the surface. In the region of the $5 \times 5\,\mathrm{nm}^2$ large filled state topograph in (a), which is taken at $I = 30\,\mathrm{pA}$ and $U = -2.2\,\mathrm{V}$, 2500 $dI/dU(U,\boldsymbol{r})$ curves are recorded. Averaged $dI/dU(U,\boldsymbol{r})$ spectra of the B atom and the GaAs surrounding are shown in (b), which are extracted from (a) in the area of the red dot and the green frame, respectively. Sections along cut lines 1 and 2 through the $dI/dU(U,\boldsymbol{r})$ map after subtraction of the GaAs background are provided in (c). A corresponding three dimensional representation of the B related differential conductance is shown in (d) using an opacity threshold of $dI/dU(U,\boldsymbol{r}) = 0.55$a. u. The origin of the spectroscopic features (I, II, and III) is sketched in the band diagrams in (e).

as an estimate for the GaAs reference spectrum. Direct comparison with the GaAs reference spectrum illustrates that the B atom enhances the differential conductance at the CBE [region (I)] and in the band gap [region (II)]. The onsets of the CB and VB, which lie at about 0.77 V and –1.12 V, are determined on the basis of the average $dI/dU(U,\boldsymbol{r})$ spectrum of the GaAs matrix in Fig. 3(b) by using a threshold of $dI/dU(U,\boldsymbol{r}) = 0.02$a. u. The experimentally observed band gap of GaAs is 24% larger than expected.[25] This is due to the tip induced band bending (TIBB), which acts especially in the nearly intrinsic epilayer region as an additional lever stretching the voltage scale.

The key to the unexpected rich spectral structure of B atoms in the surface lies in the TIBB. The bands in the semiconductor bend at growing positive voltages increasingly upwards. At some point, the Fermi level of the tip lines up with the empty B impurity state just below the CBE. However, the isolated B state does not provide a sufficiently

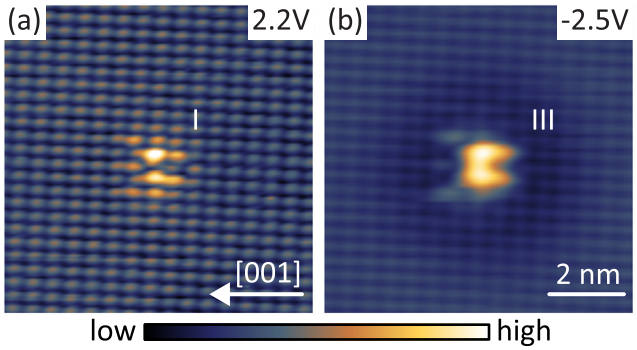

FIG. 4. High resolution topographic X-STM images of the empty (a) and filled (b) impurity state of a B atom in the surface, which are taken at $U = 2.2$ V [region (I)] and $U = -2.5$ V [region (III)]. The tunnel current is kept constant at $I = 30$ pA. The color scales in both images are adapted independently for best visibility.

large reservoir of empty states to sustain a significant tunneling path. In this configuration, no tunnel current is flowing. Only when the empty B impurity state is lifted by the TIBB to the level of the CBE far away from the surface gains, the B impurity state is relevant. This allows for resonant tunneling from the tip into the empty B impurity state and from there into the empty CB states as indicated in Fig. 3(e). Consequently, in the $dI/dU(U, \boldsymbol{r})$ spectra, region (I) coincides always with the beginning of the valence band edge (VBE). At larger positive voltages, the cationic surface states near the CBE start to contribute directly to the tunnel current. As a result, the tunneling path through the B atom loses its significance, which gives rise to the decay of the B related contributions towards larger positive voltages.

Conversely, the bands bend downwards at large negative voltages. The downward band bending ultimately causes the B impurity state to drop below the sample Fermi level. Due to the n-type nature of the sample, this is expected to occur before the Fermi level of the tip lines up with the anionic surface states in the region of the VB. Below the Fermi level of the sample, the B impurity state is always occupied and acts as a strong tunnel path into the tip. In the $dI/dU(U, \boldsymbol{r})$ spectra, this leads to a peak in the band gap (region II). Consequently, regions (I) and (II) originate from the same state, which is once occupied and once empty. Further evidence for this interpretation can be seen in the spatial congruence of the onsets of regions (I) and (II), which proves that they are both related to the anionic sublattice. Close inspection of Fig. 3(b) reveals that the B related peak in region (I) is wider and less intense than in region (II). This is attributed to the different characters of the tunneling paths in regions (I) and (II). The B impurity state aligns at positive voltages first with the CBE deep in the semiconductor. With increasing TIBB at positive voltages, the effective barrier between the B impurity state and the CB states gradually decreases. This gives rise to a gentle opening of the resonant tunneling path in region (I). The shift of the B impurity state below the Fermi level of the sample in region (II) represents a more sudden transition when compared to the onset of the resonant tunnel path in region (I), which explains the mentioned differences between regions (I) and (II).

At even larger negative voltages, the occupied surface states in the region of the valence band edge (VBE), which are located on the anionic lattice, become involved in the tunneling [see Fig. 3(e)]. Thereby, the contributions of the occupied B impurity state, which is localized on the cationic sublattice, to the total tunnel current become less important. This transition from cationic to anionic states causes the lateral shift in region (III). Furthermore, the Coulomb field of the additional charge located at the occupied B impurity state gives rise to an upwards band bending in the VB. This favors an earlier transition into the anionic surface states near the B atom than in the surrounding GaAs matrix.

High resolution filled and empty state topographs of a B atom in the surface are shown in Fig. 4, which represent the previously discussed regions I and III, respectively. These images are taken with a different tip state at another B atom in the surface than the one shown in Fig. 3(a). Therefore, the voltage set-points in the topographs cannot be directly compared with the spectroscopic data. In both cases, the B impurity state is primarily located on two neighboring lobes, which are separated from each other by an intermediate atomic row. This is in good agreement to the spectroscopic data. On the whole, a spherical symmetry prevails, as seen for donors such as Si.[26] However, there is a slight asymmetry along the [001] growth direction in the form of trident-like extensions. The buckling of the relaxed {110} surfaces runs similarly along the [001] direction, which suggests a connection between the asymmetry of the B impurity state and the surface. The B impurity state extends in the empty state X-STM image over a region of about 5×5 lattice sites. In the filled state image, the B impurity state has next to this local component an additional long ranged contribution, which appears as a halo of dark contrast. Such a behavior is typical for a perturbation of the Fermi gas by a charged defect. This gives further evidence that the B impurity state must lie below the Fermi level under filled state conditions at large negative voltages and acts as a charge carrier trap. Interestingly, the atomic corrugation in Fig. 4(b) is perpendicular to the [001] direction. However, the anionic surface states A_4 and A_5, which lie in the VB, give rise to a strong corrugation along the [001] direction. This points to contributions from the cationic C_3 surface state, which is located near the CBE. At negative sample voltages, the C_3 surface state can only contribute to the tunnel current when it is filled. Hence, the TIBB must be so strong that even the CBE lies below the Fermi level of the sample, which further supports a charged B impurity state.

This illustrates that the impurity state of a B atom in the {110} surfaces does not lie 0.3 eV above the CBE as suggested for bulk GaAs layers.[17] The spectral structure of the experimental $dI/dU(U, \boldsymbol{r})$ curves is much more indicative of a B impurity state in the band gap slightly below the CB. It is not unusual that the {110} surface affects the energetic position of the dopants.[27,28] Similar observations have been reported for highly mismatched N impurities in GaAs, which in contrast to B are located on the group V sublattice.[29]

C. Characterization of the spatial boron distribution

The considerably smaller effective size of the B atoms compared to the elements in the GaAs host makes the synthesis of borides challenging. Typical problems in the growth

of HMAs range from crystal defects to inhomogeneities in the distribution of the components, which can lead to a complete phase separation. For example, it is assumed that the unusually strong increase in the effective electron mass in B doped GaAs is related to the formation of pairs or clusters of B atoms.[30] However, supporting structure studies addressing the morphology of B-containing GaAs films at the atomic level are lacking.

Here, X-STM is used to address this topic for three different groups of B doped GaAs QWs with nominal B concentrations of 0.3% (QW 1), 0.5% (QW 2), and 1.0% (QW 3). Each of these groups consists of three sets of QWs with the same B concentrations of which always the last grown QW is examined. The classification of the main B related features in Sec. III A allows to determine the B concentration profiles in these QWs along the [001] growth direction, which are shown in Fig. 5. The concentration profile of QW 1 is calculated on the basis of B atoms in the surface layer [class (0)] and the first subsurface layer [class (1)] over a length of (360 ± 10)nm. In QWs 2 and 3, where the statistics is better, only the positions of the B atoms in the surface [class (0)] are used at a total length of (458 ± 15)nm and (478 ± 27)nm, respectively. Typical X-STM images of the last grown $B_xGa_{1-x}As$/GaAs QWs 1–3 are shown in Fig. 1 of the supplementary material.

The general tends in these three different B doped QWs are very similar. The B concentration profiles in Fig. 5 suggest a QW thickness of (14.7 ± 0.6)nm, which is in good agreement with the nominal value of 15nm. In addition, the interfaces between the neighboring GaAs barriers and the $B_xGa_{1-x}As$ wells are almost atomically sharp, which excludes B segregation. The sharp interfaces between the $B_xGa_{1-x}As$ and GaAs layers are a direct consequence of the strong B-As bond,[31] which limits the transfer of B atoms to subsequent layers during growth. For example, the weaker bound In atoms in GaAs are considerably more mobile during growth, which appears in the form of pronounced segregation patterns at the interfaces of (In, Ga)As/GaAs QWs.[32] Furthermore, the surrounding GaAs films do not show any signs of B cross contamination. The B content inside the three different barriers comes close to the intended concentrations, which are indicated by orange dashed lines. The largest deviation from the nominal B concentration is found at QW 1. This is related to the increasing difficulty in controlling low B fluxes. All

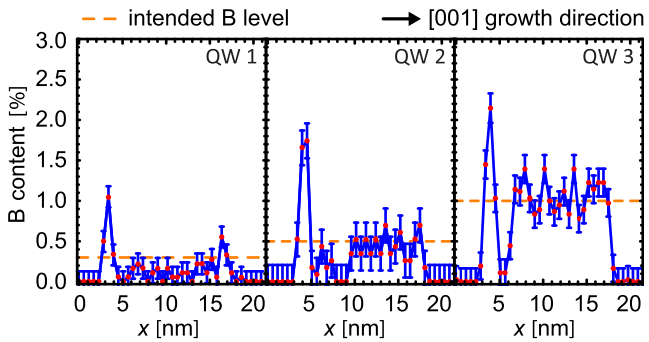

FIG. 5. Boron content along the [001] growth direction for three different $B_xGa_{1-x}As$/GaAs QWs with intended B concentrations of 0.3% (QW 1), 0.5% (QW 2), and 1.0% (QW 3).

this suggests good control over the incorporation of B atoms in GaAs. However, the B distribution shows a very particular behavior at the growth start of every B-containing GaAs QW. There seems to be a B-rich δ-layer, which is followed by a region where almost no B atoms are found. This is induced by unintentional instabilities in the B pressure at the beginning of the QW growth, which affects the incorporation of B atoms in the GaAs matrix.

To assess the short range ordering of the B atoms relative to each other, the occurrence of the n-th nearest neighbor B pairs with $n = 1, 2, 3, 4$, and 6 in the cleaved {110} surfaces is investigated. The fifth nearest neighbor pair is not considered as it cannot be found in the {110} planes. QWs 3, which have the highest B concentration and thus the highest density of B pairs, are best suited for studying the occurrence of the B pairs. Here, the number of B pairs is visually determined over a length of (478 ± 27)nm for each of the three QWs 3 with a B concentration of 1%. Examples of the B pairs under filled state conditions and their orientation in the surface are shown in Figs. 6(c) and 6(b). Surprisingly, we

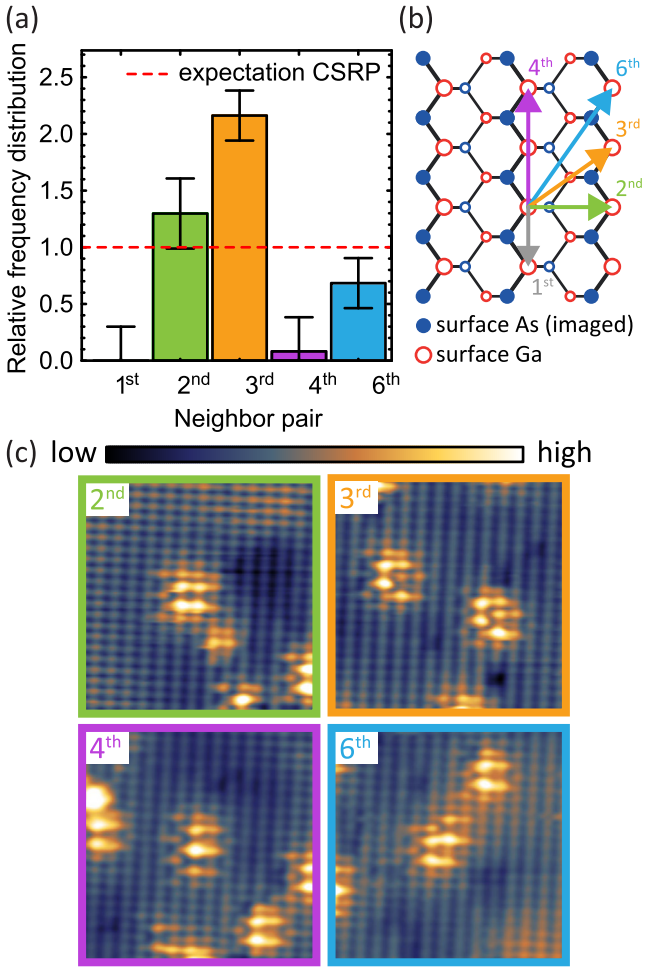

FIG. 6. Relative frequency distribution (a) of the n-th nearest neighbor B pairs in the cleavage plane with $n = 1, 2, 3, 4$, and 6, which is derived over a length of (478 ± 27)nm from each of the three QWs 3 with a B concentration of 1%. A model of the (110) surface is shown in (b), where the orientations of the investigated n-th nearest neighbor B pairs are marked. Corresponding filled state images of the observed n-th nearest neighbor B pairs in the cleavage plane are shown in (c), which are taken at $I = 40$ pA and $U = -2.5$V.

did not find any first nearest neighbor B pairs. The experimentally observed numbers of B pairs are normalized by the expectations for a completely spatially random pattern (CSRP). This results in the relative frequency distribution in Fig. 6(a), which gives a direct measure for the deviation of the experimental B pair distribution from the ideal case of a CSRP. The number of B pairs, which are expected for a CSRP, are estimated from 10 000 computationally generated patterns where B atoms are randomly distributed across atomic grids with the same dimensions and B concentration profiles as in the experimentally studied QWs 3. In this way, deviations from the ideally rectangular B concentration profile, which are an artifact of the growth procedure, are considered. The statistical error of the experimental B pair counts is estimated on the basis of the standard deviation of the simulated CSRPs.

The relative frequency distribution in Fig. 6(a) shows that there is not only a strong underpopulation of the first and fourth nearest neighbor pairs, but also a clear overpopulation of the third nearest neighbor pairs. In fact, we found no first and only one fourth nearest neighbor B pair in the whole investigated region. This is, in both cases, a deviation from the reference level of a CSRP by more than two standard deviations. Similarly, the third nearest neighbor pairs are observed more than twice as often than expected for a CSRP. It appears likely that the lack of B atoms on the first and fourth nearest neighbor position and the surplus on the third nearest neighbor positions are related. In this context, it is interesting to note that both the first and fourth nearest neighbor pairs are oriented along the directly coupled zigzag rows of Ga and As atoms in the $\langle 110 \rangle$ directions.

The reduced number of first and fourth nearest neighbor pairs, as well as the increased occurrence of the third nearest neighbor pairs could be related to an exchange of B and Ga atoms in the cleaved {110} surfaces after the growth. However, extensive X-STM studies in the last decades on III-V semiconductor compounds have shown that *in situ* cleaved {110} surfaces are very stable under UHV conditions. In addition, the B-V bonds belong in the III-V system to one of the strongest.[31] Only the wide band gap III-N compounds have stronger binding energies. Therefore, it appears unlikely that the deviation of the local B distribution from a CSRP is induced by the X-STM measurement. This leaves only the possibility of a growth related mechanism.

Up to now, the B first nearest neighbor pairing is considered as the main cause for the unusually strong increase in the CB effective mass in boride III-V compounds.[13] This belief goes back to the theoretical work of Lindsay *et al.* in Ref. 30 on the band structure of B doped GaAs. Their TB calculations indicated that the strong increase in the CB effective mass is related to the first nearest neighbor B pairing, which affects the CBE much stronger than individual B atoms. Our study points to an intrinsic mechanism during growth, which strongly suppresses the formation of the first and fourth nearest neighbor B pairs in the investigated sample at a B concentration of 1%. This suggests that the extraordinary increase in the CB effective mass, which is reported for boride III-V semiconductors, may not be attributed to the B first nearest neighbor paring in the transition region between a dilute system and an alloy.[15,17,30] Further work is needed to clarify whether the observed deviations in the spatial B distribution from a CSRP in QWs 3 with a B concentration of 1% prevail also at lower and higher amounts of B atoms.

IV. CONCLUSION

X-STM is used to explore the structural and electronic properties of B atoms in GaAs, which have until now largely been disregarded in the III-V material system. The increasing interest in the small B atoms as an isovalent impurity in conventional binary III-V semiconductors arises in the search for novel materials, which, similar to dilute nitrides and bismides, offer new functionalities.

Boron atoms on substitutional Ga sides are identified down to the second layer below the natural {110} cleavage planes. The contrast of B atoms in subsurface layers is primarily given by the local deformation of the surrounding GaAs matrix towards the smaller B atoms. Surprisingly, boron atoms in the cleavage plane give rise to strong electronic signatures. This is a direct consequence of the surface, which affects the energetic position of the B impurity state. Usually, boron introduces in GaAs an impurity state, which is resonant with the CB. However, our scanning tunneling spectroscopy (STS) measurements show that the impurity state of a B atom in the GaAs {110} surface lies just below the CBE, which dominates the contrast in topographic X-STM images. Taking advantage of the TIBB in the tunnel junction, the filled and empty impurity states of the same B atom in the surface are imaged.

In addition, the structural properties of different $B_xGa_{1-x}As/GaAs$ QWs are investigated. Along the [001] growth direction, the incorporation of B atoms in GaAs can be controlled at the atomic level. This is attributed to the strong B-As bond, which limits the segregation rate of the B atoms. In general, the crystal quality of the B-containing GaAs layers is very good with no indications of crystal defects in the investigated concentration range from 0.3% to 1.0%. However, at a B concentration of 1%, a lack of first and fourth nearest neighbor B pairs compared to a CSRP is found. At the same time, third nearest neighbor B pairing appears to be much more favorable than in a CSRP.

SUPPLEMENTARY MATERIAL

See supplementary material for high resolution X-STM images, which provide an overview of the investigated $B_xGa_{1-x}As/GaAs$ QWs with B concentrations of 0.3% (QW 1), 0.5% (QW 2), and 1.0% (QW 3).

ACKNOWLEDGMENTS

C.M.K. and P.M.K. thank NanoNextNL, a micro and nanotechnology consortium of the Government of the Netherlands and 130 partners, for the financial support. L.N., E.S., and K.V. gratefully acknowledge the support from the German Research Foundation (DFG) in the framework of the RTG1782 "Functionalization of Semiconductors."

[1]J. Wu, W. Shan, and W. Walukiewicz, Semicond. Sci. Technol. **17**, 860 (2002).
[2]K. Alberi, J. Wu, W. Walukiewicz, K. M. Yu, O. D. Dubon, S. P. Watkins, C. X. Wang, X. Liu, Y.-J. Cho, and J. Furdyna, Phys. Rev. B **75**, 045203 (2007).
[3]S. Francoeur, G. Sivaraman, Y. Qiu, S. Nikishin, and H. Temkin, Appl. Phys. Lett. **72**, 1857 (1998).
[4]W. Shan, W. Walukiewicz, K. M. Yu, J. Wu, J. W. Ager III, E. E. Haller, H. P. Xin, and C. W. Tu, Appl. Phys. Lett. **76**, 3251 (2000).
[5]W. G. Bi and C. W. Tu, J. Appl. Phys **80**, 1934 (1996).
[6]S. Francoeur, M.-J. Seong, A. Mascarenhas, S. Tixier, M. Adamcyk, and T. Tiedje, Appl. Phys. Lett. **82**, 3874 (2003).
[7]S. P. Svensson, H. Hier, W. L. Sarney, D. Donetsky, D. Wang, and G. Belenky, J. Vac. Sci. Technol., B **30**, 02B109 (2012).
[8]K. Wang, Y. Gu, H. F. Zhou, L. Y. Zhang, C. Z. Kang, M. J. Wu, W. W. Pan, P. F. Lu, Q. Gong, and S. M. Wang, Sci. Rep. **4**, 5449 (2014).
[9]J. Kopaczek, R. Kudrawiec, M. P. Polak, P. Scharoch, M. Birkett, T. D. Veal, K. Wang, Y. Gu, Q. Gong, and S. Wang, Appl. Phys. Lett. **105**, 222104 (2014).
[10]P. Pyykkö and M. Atsumi, Chem.: Eur. J. **15**, 186 (2009).
[11]G. Leibiger, V. Gottschalch, V. Riede, M. Schubert, J. N. Hilfiker, and T. E. Tiwald, Phys. Rev. B **67**, 195205 (2003).
[12]W. Shan, W. Walukiewicz, J. Wu, K. M. Yu, J. W. Ager III, S. X. Li, E. E. Haller, J. F. Geisz, D. J. Friedman, and S. R. Kurtz, J. Appl. Phys. **93**, 2696 (2003).
[13]T. Hofmann, M. Schubert, G. Leibiger, and V. Gottschalch, Appl. Phys. Lett. **90**, 182110 (2007).
[14]G. L. W. Hart and A. Zunger, Phys. Rev. B **62**, 13522 (2000).
[15]J. Teubert, P. J. Klar, A. Lindsay, and E. P. O'Reilly, Phys. Rev. B **83**, 035203 (2011).
[16]L. Ostheim, P. J. Klar, S. Liebich, P. Ludewig, K. Volz, and W. Stolz, Semicond. Sci. Technol. **31**, 07LT01 (2016).
[17]S. Petznick, L. Ostheim, P. J. Klar, S. Liebich, K. Volz, and W. Stolz, Appl. Phys. Lett. **105**, 222105 (2014).
[18]P. Ebert, B. Engels, P. Richard, K. Schroeder, S. Blügel, C. Domke, M. Heinrich, and K. Urban, Phys. Rev. Lett. **77**, 2997 (1996).
[19]F. J. Tilley, M. Roy, P. A. Maksym, P. M. Koenraad, C. M. Krammel, and J. M. Ulloa, Phys. Rev. B **93**, 035313 (2016).
[20]C. M. Krammel, M. Roy, F. J. Tilley, P. A. Maksym, L. Y. Zhang, P. Wang, K. Wang, Y. Y. Li, S. M. Wang, and P. M. Koenraad, Phys. Rev. Mater. **1**, 034606 (2017).
[21]H. A. McKay, R. M. Feenstra, T. Schmidtling, and U. W. Pohl, Appl. Phys. Lett. **78**, 82 (2001).
[22]H. A. McKay, R. M. Feenstra, T. Schmidtling, U. W. Pohl, and J. F. Geisz, J. Vac. Sci. Technol. B **19**, 1644 (2001).
[23]J. M. Ulloa, P. M. Koenraad, and M. Hopkinson, Appl. Phys. Lett. **93**, 083103 (2008).
[24]A. P. Wijnheijmer, O. Makarovsky, J. K. Garleff, L. Eaves, R. P. Campion, B. L. Gallagher, and P. M. Koenraad, Nano Lett. **10**, 4874 (2010).
[25]I. Vurgaftman, J. R. Meyer, and L. R. Ram-Mohan, J. Appl. Phys. **89**, 5815 (2001).
[26]J. F. Zheng, X. Liu, N. Newman, E. R. Weber, D. F. Ogletree, and M. Salmeron, Phys. Rev. Lett. **72**, 1490 (1994).
[27]A. P. Wijnheijmer, J. K. Garleff, K. Teichmann, M. Wenderoth, S. Loth, R. G. Ulbrich, P. A. Maksym, M. Roy, and P. M. Koenraad, Phys. Rev. Lett. **102**, 166101 (2009).
[28]P. Kloth and M. Wenderoth, Sci. Adv. **3**, e1601552 (2017).
[29]N. Ishida, M. Jo, T. Mano, Y. Sakuma, T. Noda, and D. Fujita, Nanoscale **7**, 16773 (2015).
[30]A. Lindsay and E. P. O'Reilly, Phys. Rev. B **76**, 075210 (2007).
[31]P. Manca, J. Phys. Chem. Solids **20**, 268 (1961).
[32]K. Muraki, S. Fukatsu, Y. Shiraki, and R. Ito, Appl. Phys. Lett. **61**, 557 (1992).